AIAA JOURNAL
Vol. 31, No. 4, April 1993

Grid-Independent Upwind Scheme for Multidimensional Flow

Ijaz H. Parpia* and Donna J. Michalek†
University of Texas at Arlington, Arlington, Texas 76019

Recent advances in the development of a grid-independent finite volume scheme for the Euler equations of gas dynamics are described. In the proposed method, flowfield gradient data are reconstructed locally (on a triangle) using five elementary planar waves, and an upwind numerical flux function for grid-oblique waves is developed to model the effect of the passage of these waves on the data in a cell. Numerical examples for several two-dimensional test problems are included. These results show high wave resolution and nearly monotone strong-wave transitions.

I. Introduction

THERE have been several recent studies on a family of genuinely multidimensional finite-volume algorithms in which wave strength and orientation information is derived from two neighboring states.[1-4] These methods are designed specifically to "recognize" single Rankine-Hugonoit wave transitions, and where the data fail to indicate the presence of a single wave, a plausible set of waves derived from various rules of thumb is used to reconstruct the jump between the states. The success of this approach has been quite limited, perhaps because it is simply unreasonable to suppose that two states can provide a realistic account of the local wave content of the flowfield.

In this paper we describe the development of an algorithm for two-dimensional flow in which a third data point is introduced into the local reconstruction. Planar wave solutions of the Euler equations are superposed to reconstruct an estimate of the flowfield gradients on a triangle.[5] Because the wave orientation and propagation directions are derived from the gradient data, rather than from the cell geometry, the method is called "grid independent."

In the next section we describe the numerical method. Several test cases are presented in Sec. III, and we discuss the performance of the new method and issues for future research in Sec. IV.

II. Numerical Method

Unstructured Discretization

A three-state local reconstruction of the data fits naturally into the standard unstructured mesh discretization, in which the region of interest is divided into a set of nonoverlapping triangles. The grids used in Sec. III were generated by a Delaunay node generation and triangulation procedure developed by Hase et al.[6]

The flow solver described in this paper is node centered, with computational cells built from the triangle-centroid mesh dual shown in Fig. 1. Each face of any polygonal cell is shared by adjacent triangles in the patch surrounding a node, and the wave model, together with the flux formula described later, is used to write a numerical approximation to the flux on every half-face (the portion of the face contained in a triangle).

Planar Wave Solutions

The Euler system can be written in the quasilinear form

$$\frac{\partial V}{\partial t} + A\frac{\partial V}{\partial x} + B\frac{\partial V}{\partial y} = 0$$

where $V = (\rho, u, v, p)$ is the vector of primitive variables (density, particle velocity, and pressure). Elementary solutions of this system of equations are of the form

$$V(x, t) = \alpha(n)e(n)\ (x \cdot n - \lambda t) \tag{1}$$

Equation (1) defines a wave of strength α, with wave front normal n and wave speed λ; e is the eigenvector that describes the transition across the wave in state space. These elementary solutions define three families of solutions: acoustic, shear, and entropy waves. It is our intention to use these waves as building blocks in the local description of the flow properties.

For computational simplicity, we define a local linearization of the governing equations, in which we replace the coefficient matrices A and B with constant matrices $\hat{A}$ and $\hat{B}$ and then reconstruct the data using superposition. One such linearization procedure is Roe averaging,[7] which has proved to be remarkably effective in classical grid-aligned methods and is also central to the recently developed multidimensional fluctuation splitting algorithm of Struijs et al.[8] We use a different linearization here, following the Rankine-Hugoniot averaging technique,[9] which is described in an earlier paper.[4]

The eigenvectors $\hat{e}$ and wave speeds of $\hat{\lambda}$ of the Rankine-Hugoniot linearized equations are

$$\hat{e}_{ac} = \begin{bmatrix} \bar{\rho}/(\gamma\bar{p}) \\ \pm\psi/\hat{a}n_x^{ac} \\ \pm\psi/\hat{a}n_y^{ac} \\ 1 \end{bmatrix}, \quad \hat{e}_{sh} = \begin{bmatrix} 0 \\ -n_y^{sh} \\ n_x^{sh} \\ 0 \end{bmatrix}, \quad e_{en} = \begin{bmatrix} 1 \\ 0 \\ 0 \\ 0 \end{bmatrix} \tag{2}$$

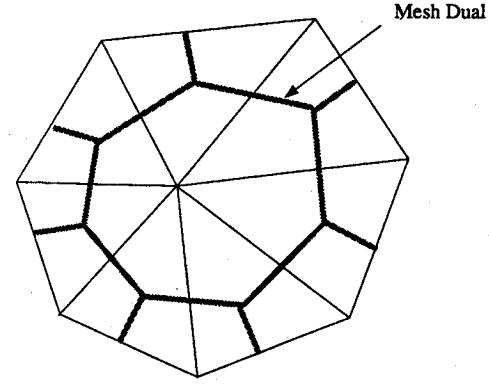

Fig. 1 Finite volume cell.

Presented in part as Paper 92-0325 at the AIAA 30th Aerospace Sciences Meeting, Reno, NV, Jan. 6-9, 1992; received March 23, 1992; revision received Aug. 5, 1992; accepted for publication Aug. 12, 1992.

*Assistant Professor, Department of Aerospace Engineering. Member AIAA.

†Graduate Student, Department of Aerospace Engineering.

and

$$\hat{\lambda}_{ac} = \bar{u} \cdot n^{ac} \pm \hat{a}$$
$$\hat{\lambda}_{sh} = \bar{u} \cdot n^{sh} \tag{3}$$
$$\hat{\lambda}_{en} = \bar{u} \cdot n^{en}$$

where the overbar denotes an arithmetic average, $\psi = \overline{1/\rho}$, and the Rankine-Hugoniot averaged speed of sound is $\hat{a} = \sqrt{\gamma \bar{p} \psi}$.

Wave Model

In the classical approach to upwinding in several space dimensions, the transition between any two neighboring states on the computational grid is assumed to be described by waves that are aligned with the finite volume cell faces. There are four waves in two space dimensions and five in three. The wave strengths are the free parameters and are chosen to match the given transition.

We abandon the grid-aligned wave approach and instead use local flowfield data to deduce the wave orientations. This has been done using a variety of wave models.[1-5,8,10]

The transition between two adjacent states is perhaps best interpreted according to the closest single-wave description, and we and others have had limited success with this approach.[1-4] We have found that a far more robust method results if the support for the reconstruction includes a third data point. For this reason, we seek a wave description of the data on a triangle. The variations described by the wave pattern are chosen to match the data, which provide approximations to the eight components of the gradient of the dependent variables. One might suppose that the minimum number of waves necessary to do this in two dimensions is four (each wave has two free parameters, strength and orientation), but no choice of four waves can describe general data. A study of the eigenvectors (2) shows that the minimum number of waves is in fact five, consisting of two acoustics, two shears, and an entropy wave, and this is the choice we make in the algorithm described later. Noting that only eight wave parameters follow from the data, we are at liberty to specify two quantities in a five-wave model of this type, with the conditions that the solution for the remaining parameters exists, is real valued, and can be obtained efficiently.[5]

We specify that the acoustic waves be a forward and backward facing pair with common normal n^{ac} and that the two shear waves be mutually perpendicular, with normals n^{sh_1} and n^{sh_2}. The entropy wave normal is n^{en}. The system of eight equations from which the unknown wave parameters are found is

$$\nabla p = (\beta_{ac_1} + \beta_{ac_2})\, n^{ac} \tag{4}$$

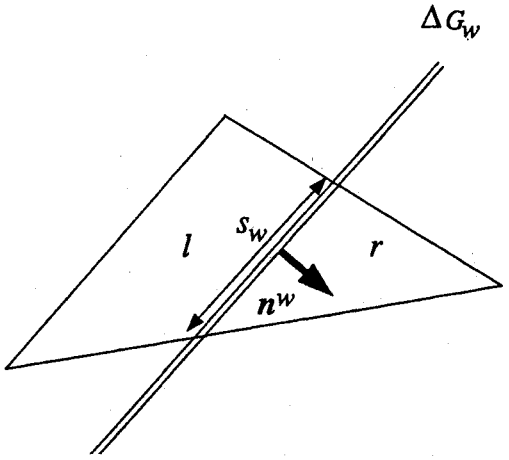

Fig. 2 Plane wave moving through a triangular cell fragment.

$$\nabla \rho = \beta_{en} n^{en} + \frac{\bar{\rho}}{\gamma \bar{p}} (\beta_{ac_1} + \beta_{ac_2}) n^{ac} \tag{5}$$

$$u_x = -\beta_{sh_1} n_y^{sh_1} n_x^{sh_1} - \beta_{sh_2} n_y^{sh_2} n_x^{sh_2} + \frac{\psi}{\hat{a}} (\beta_{ac_1} - \beta_{ac_2})(n_x^{ac})^2 \tag{6}$$

$$u_y = -\beta_{sh_1} (n_y^{sh_1})^2 - \beta_{sh_2} (n_y^{sh_2})^2 + \frac{\psi}{\hat{a}} (\beta_{ac_1} - \beta_{ac_2}) n_x^{ac} n_y^{ac} \tag{7}$$

$$v_x = \beta_{sh_1} (n_x^{sh_1})^2 + \beta_{sh_2} (n_x^{sh_2})^2 + \frac{\psi}{\hat{a}} (\beta_{ac_1} - \beta_{ac_2}) n_y^{ac} n_x^{ac} \tag{8}$$

$$v_y = \beta_{sh_1} n_x^{sh_1} n_y^{sh_1} + \beta_{sh_2} n_x^{sh_2} n_y^{sh_2} + \frac{\psi}{\hat{a}} (\beta_{ac_1} - \beta_{ac_2})(n_y^{ac})^2 \tag{9}$$

All of the averages in these equations are triangle averages, and β denotes a wave strength per unit length across the wave (in the direction of the wave normal). The solution of this system of equations can be obtained easily. The acoustic and entropy wave normals are

$$n^{ac} = \frac{\nabla p}{|\, \nabla p \,|} \tag{10}$$

and

$$n^{en} = \frac{\nabla \rho - \bar{\rho}/(\gamma \bar{p}) \nabla p}{|\, \nabla \rho - \bar{\rho}/(\gamma \bar{p}) \nabla p \,|} \tag{11}$$

the shear wave angles are

$$\theta_{sh_1} = \tfrac{1}{2} \arctan \left[\frac{(v_y - u_x) - \cos 2\theta_{ac}(u_x + v_y)}{(v_x + u_y) + \sin 2\theta_{ac}(u_x + v_y)} \right]$$
$$= \tfrac{1}{2} \arctan \frac{N}{D} \qquad \theta_{sh_2} = \theta_{sh_1} + \frac{\pi}{2} \tag{12}$$

and the wave strengths are

$$\beta_{ac_{1,2}} = \frac{1}{2} \left(|\, \nabla p \,| \pm \frac{\hat{a}}{\psi} \nabla \cdot u \right) \tag{13}$$

$$\beta_{en} = |\, \nabla \rho - \bar{\rho}/(\gamma \bar{p}) \nabla p \,| \tag{14}$$

$$\beta_{sh_{1,2}} = \tfrac{1}{2} [(v_x - u_y) \mp (D \cos 2\theta_{sh_1} + N \sin 2\theta_{sh_1})] \tag{15}$$

By construction, the wave model described earlier provides an accurate wave decomposition of any flow that is dominated by wave interactions of the type we have assumed. In particular, the model returns an accurate description of a flow that is dominated by a single oblique wave. But because an infinite variety of flows can produce the same gradient data on the triangle, no method of the type we have presented can give the "correct" description of an arbitrary flow. At points where the model fails to be valid, we rely on the wave model appropriately incorporated into an upwind flux formula (described later) to provide sufficient dissipation for the algorithm to be robust over a useful range of problems. Of course, the basic requirement that the scheme be conservative must be met in any case.

It is possible to write analogous wave decompositions of three-dimensional data, where 15 free wave parameters must be matched to the gradient; Roe has presented such a method.[5] As in the two-dimensional case, it would appear that the utility of any wave model will ultimately be decided by the success that attends its application to a variety of flow problems.

Flux Formula

Suppose that the finite volume cell shown in Fig. 1 is assembled from a set of triangles that are constructed by connecting the vertices of the polygonal cell to the center node. Such a

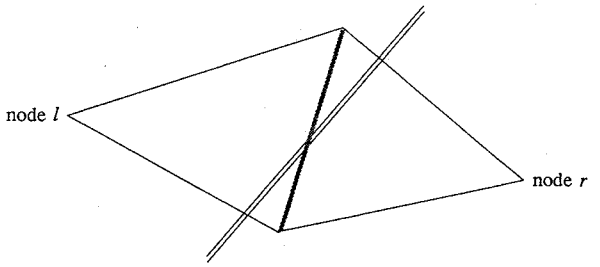

Fig. 3 Neighboring triangular cell fragments.

triangle is shown in Fig. 2. We now imagine a single plane wave front passing through this triangle. Let the state ahead of the wave be denoted by the subscript r and that behind the wave by l. The contour integral of the normal component of the flux tensor around the cell gives the simple result

$$\frac{\partial}{\partial t}(\bar{Q}A) = -s_w \Delta G_w \tag{16}$$

where $\bar{Q}$ is the area-averaged value of the vector of conserved variables (mass, momentum, and energy per unit area), A is the area of the triangle, s_w is the length of the wave front inside the triangle, and ΔG_w is the *normal* flux jump across the wave.

Figure 3 depicts two triangular fragments of neighboring cells l and r. For algorithmic simplicity, we wish to account for the entire effect of the waves that arise between the states l and r through the numerical flux at the common face. This would obviate the need to explicitly calculate the effect of these waves on the remaining faces of the triangular segments. The manner in which this can be accomplished is to set the flux at the common face, normal to the face, to

$$F = F_l + \Delta G_w \frac{s_w^l}{s_f} \tag{17}$$

where s_w^l is an estimate of the length of the wave segment contained in the left triangle, and s_f is the face length. We note that it is equally valid to write

$$F = F_r - \Delta G_w \frac{s_w^r}{s_f} \tag{18}$$

and it is perhaps most reasonable to use the average of Eqs. (17) and (18). Finally, for simplicity, we assume that the ratio of the length of the wave segment to the cell face length is zero or unity, depending on the direction of motion of the wave. This yields the flux formula

$$F = \frac{1}{2}\left[F_l + F_r - \sum_{w=1}^{5} \operatorname{sgn}(\lambda_w)\Delta G_w\right] \tag{19}$$

for a system of five waves.

The normal flux jumps ΔG_w that appear in the flux formula (19) are estimated by projecting the triangle-based wave system onto the relevant edge of the triangle and then assuming that the transition on this edge due to a given distributed wave occurs across a single wave of the same integrated strength α_w. Suppose τ is the directed line segment between nodes l and r. Then

$$\alpha_w = \beta_w \boldsymbol{n}^w \cdot \boldsymbol{\tau} \tag{20}$$

and with α_w defined in this way, the normal flux jump is taken to be

$$\Delta G_w = \alpha_w \hat{\lambda}_w \hat{\boldsymbol{e}}_w \tag{21}$$

This relation shows that upwinding is incorporated into the flux formula through terms that depend linearly on the length of the triangle side $|\tau|$. The formula (19) is, therefore, no better than first-order accurate.

Boundary Conditions

A consistent treatment of the boundaries in a grid-independent scheme would require that the wave model be altered fundamentally and in a manner that is consistent with the type of boundary. We might, for instance, use a wave pattern that would more faithfully model wave reflection. Our research in this area is not satisfactorily complete. For this reason, we rely on boundary treatments that have been widely applied in traditional grid-aligned wave schemes. A provisional solution is computed at a boundary cell assuming that no wave emanates from the boundary faces, and simple waves propagating normal to the boundary faces then provide the corrections necessary to satisfy the boundary conditions.[11]

III. Implementation

The algorithm developed earlier has been tested on a number of planar flow problems. The array of test cases discussed next consists of two supersonic channel flows, a pure supersonic shear flow, and a subsonic channel flow. A two-step predictor-corrector time integration scheme with local time stepping at a Courant-Friedricks-Lewy (CFL) number of 0.7 is used in every case.

A time study on a Sun 3/260 workstation has indicated that the low-order grid-independent scheme is about 20–30% slower than the low-order grid-aligned scheme. It should be kept in mind that this comparison was made on research versions of the two codes.[12]

Supersonic Channel Flow

This is the problem of Levy et al.[10] The lower wall of the channel consists of two flat regions connected by a 15-deg ramp, as shown in Fig. 4. The 1074-node mesh, used in all of the calculations presented for this problem, is also shown in this figure.

A baseline solution for an inflow Mach number of 2 was computed using the high-order grid-aligned scheme developed by Barth and Jesperson,[13] with least squares linear reconstruction of the data.[14] The general features of the flowfield are readily apparent in the plot of Mach number contours shown in Fig. 5.

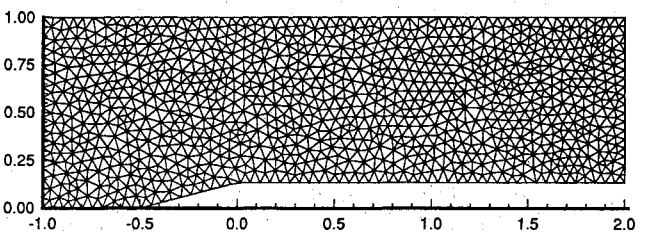

Fig. 4 Grid for the supersonic channel flow.

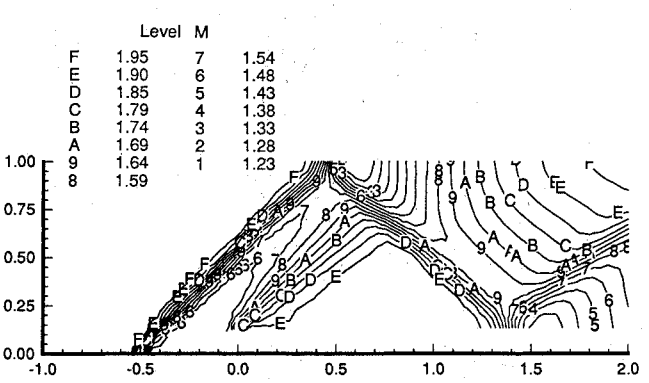

Fig. 5 Mach number contours, high-order grid-aligned scheme.

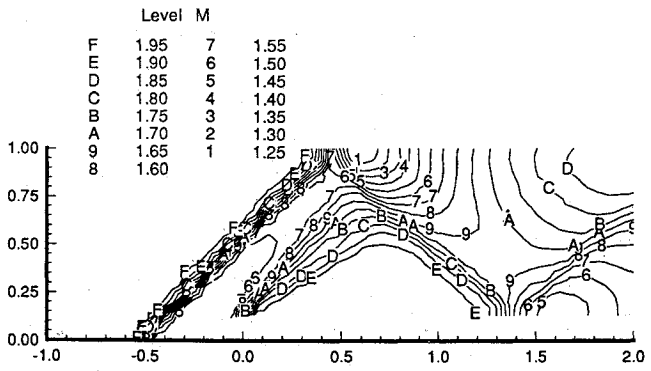

Fig. 6 Mach number contours, low-order grid-independent scheme.

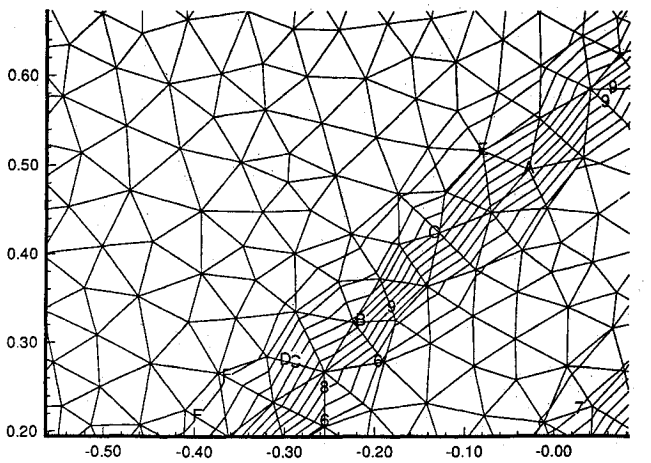

Fig. 7 Mach number contours, low-order grid-independent scheme (detail).

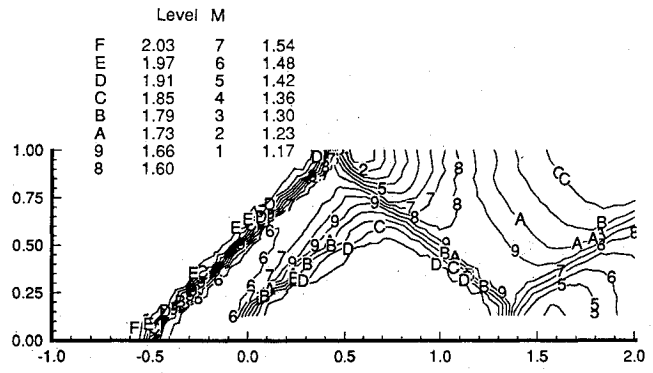

Fig. 8 Mach number contours, low-order, two-state reconstruction scheme.

Mach numbers contours for the low-order implementation of the grid-independent scheme described in this paper are shown in Fig. 6. Taken together, the data in Figs. 5 and 6 indicate that the grid-independent scheme provides resolution of the shock structures that is comparable to the high-order grid-aligned scheme. In both cases, the shock transitions are monotonic, and the resolution of the shock waves is generally good (2–3 triangles). This is confirmed in Fig. 7, which is a close-up view of the mesh overlaid onto the Mach number contours of Fig. 6 in a region around the wedge shock.

A plot of the solution using an implementation of a four-wave, two-state reconstruction scheme[4] on an unstructured grid is given in Fig. 8. This plot shows the nonmonotone behavior we have seen using two-state reconstruction schemes. The maximum Mach number ahead of the wedge shock is 2.092. Furthermore, the convergence of a method of this type is poor. The density residual diminishes by about one order of magnitude over 800 time steps.

For completeness, we also show a low-order grid-aligned result in Fig. 9. The poor resolution of weak to moderate strength waves apparent in this plot is quite typical of first-order accurate methods. The improvement that oblique-wave reconstruction provides is made dramatically clear by comparing Fig. 6 with Fig. 9.

The density residual history, shown in Fig. 10, indicates a three order-of-magnitude convergence in about 800 steps, after which the residual begins to oscillate. It appears that this problem arose due to insufficient damping of the feedback of small oscillations in the wave parameters to the flux formula.

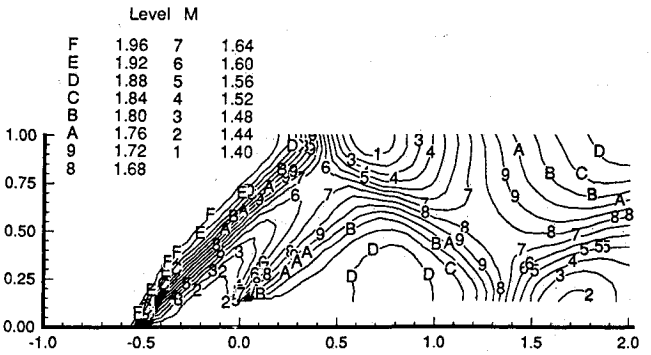

Fig. 9 Mach number contours, low-order grid-aligned scheme.

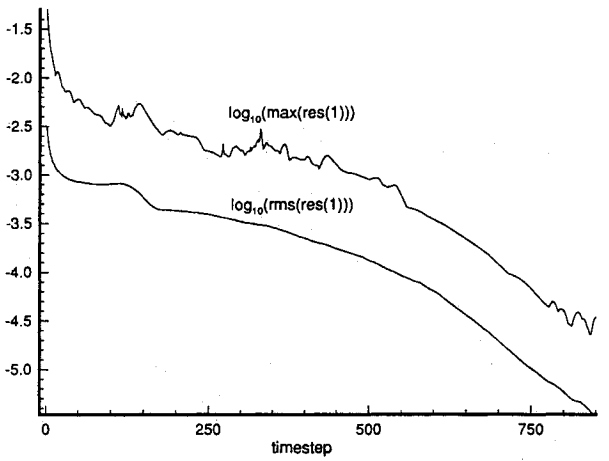

Fig. 10 Density residual history, present method.

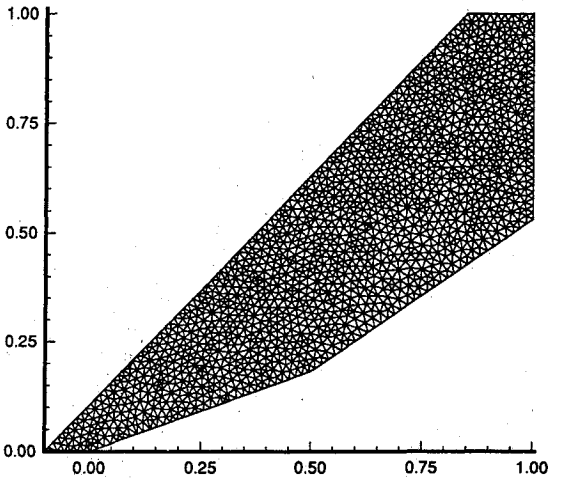

Fig. 11 Grid for the double ramp.

Double Ramp

The monotonicity and convergency behavior of the scheme is tested far more severely in this flowfield, which is a Mach 4 flow over a 20–35 deg double ramp. The uniform 1603 node grid we used is shown in Fig. 11.

Mach number contours are shown in Fig. 12. A survey of the flowfields shows that the maximum value of the Mach number ahead of the leading shock is 4.007, indicating that the solution is not strictly monotonic. We note, however, that this nonmonotonic behavior is far less severe than is typical of solutions computed using two-state reconstruction schemes.

The resolution of the shock layer is improved considerably by the grid-independent treatment, as is shown in Fig. 13, which is a plot of the Mach number distribution across the shock layer at $x = 0.85$.

The loss of monotonicity in the solution is accompanied by a slight deterioration in the convergence behavior, as is shown in the density residual history plot, Fig. 14.

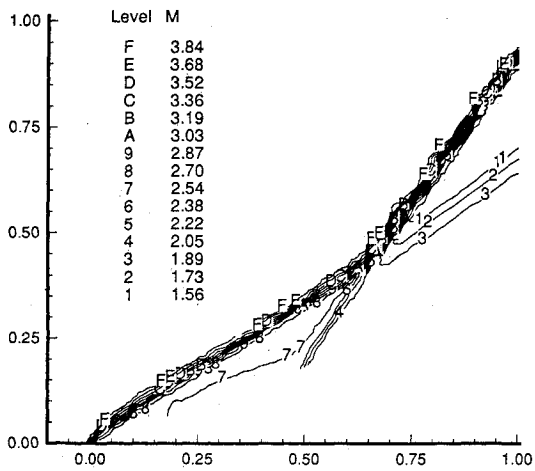

Fig. 12 Mach number contours, present method.

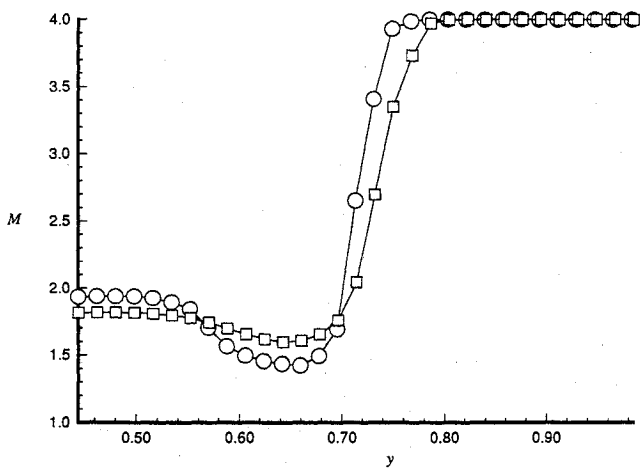

Fig. 13 Mach number variation across the shock layer, $x = 0.85$; circles: present scheme, squares: low-order grid-aligned scheme.

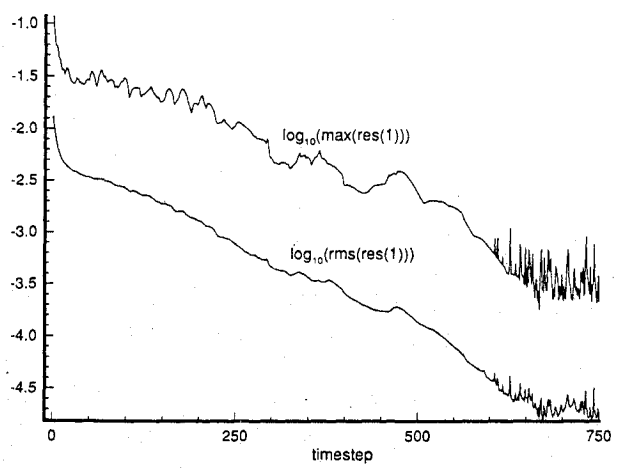

Fig. 14 Density residual history, present method.

Supersonic Shear Flow

This is a 45-deg shear layer across which the Mach number jumps from 2 to 3. The uniform 655 node grid used in this case is shown in Fig. 15. The initial conditions we used were uniform Mach 3 flow at 45 deg in the interior, with a perfectly resolved shear at the lower boundary. The side and top boundaries are freestream boundaries.

Although it might appear at first sight that a flow of this type would be a "sitting duck" for a scheme based on an oblique-wave reconstruction, it is important to note that noise in the solution can have a significant effect on resolution. Equation (12) shows that noise in the pressure and dilation

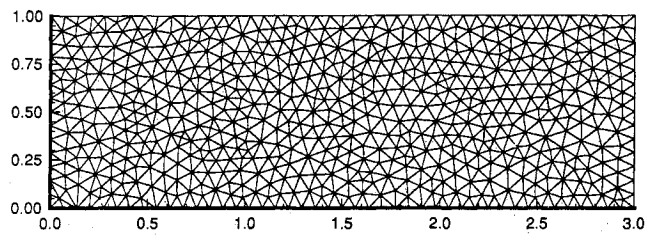

Fig. 15 Grid for the shear flow.

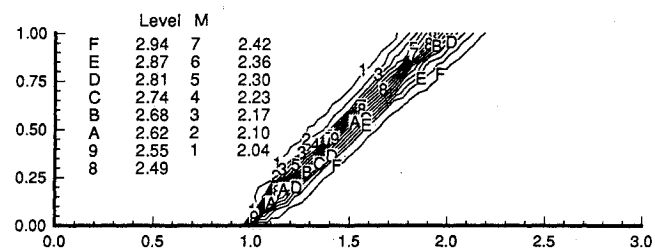

Fig. 16 Mach number contours, present method.

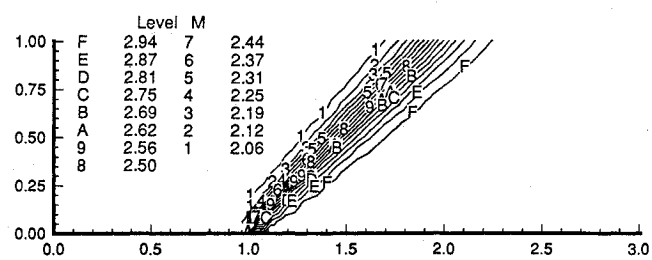

Fig. 17 Mach number contours, high-order grid-aligned scheme.

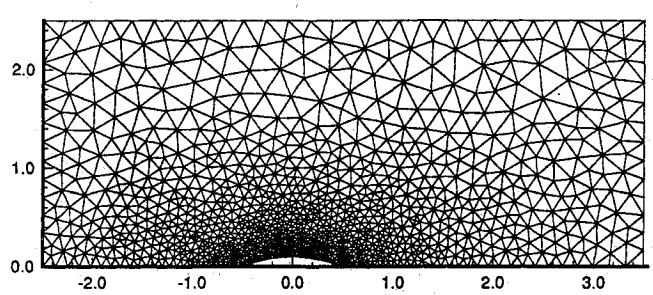

Fig. 18 Grid for the subsonic channel flow.

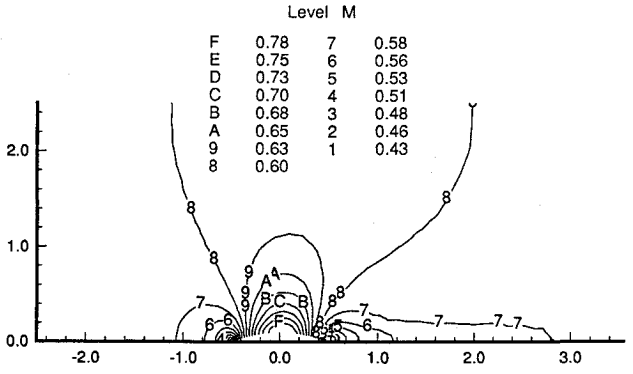

Fig. 19 Mach number contours, present method.

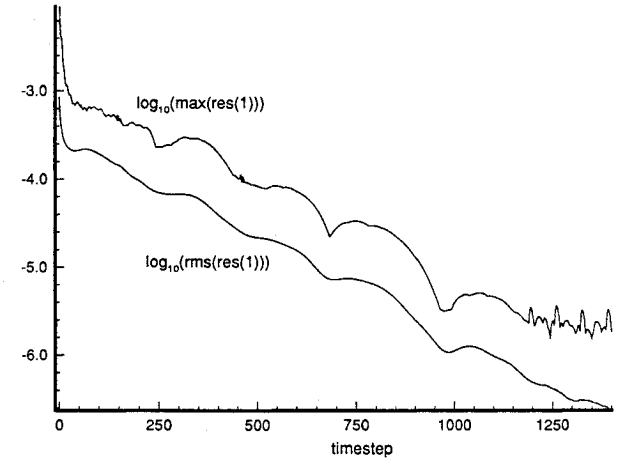

Fig. 20 Density residual history, present method.

fields has a direct effect on the computed shear angle. As is well known, a shear wave is particularly vulnerable to small errors because there is no steepening mechanism to fight the tendency of the wave to spread.

The Mach number contours shown in Fig. 16 indicate that the wave has spread across 5–6 triangles at the upper boundary, which compares very well with the high-order grid-aligned solution shown in Fig. 17.

Subsonic Channel Flow

It has been observed that there is sometimes a rapid deterioration in solution quality when grid-independent methods are applied to fully subsonic flow problems, and in fact there are schemes that fail completely in some cases.[8] These difficulties can be traced back to the central theme in the wave decomposition approach. If the wave reconstruction depends heavily on the existence of dominant wave components in the data, it follows that the lack of strongly preferred directions can lead to a failure of the method. By the same line of reasoning, it would appear that even a robust oblique-wave decomposition procedure would give little improvement in solution resolution over a grid-aligned wave decomposition. The results presented here for subsonic channel flow are consistent with this observation.

The lower wall of the channel shown in Fig. 18 is a 10% circular arc. The stretched grid contains a total of 1102 nodes, and there are 29 nodes on the bump. Mach number contours for an inflow Mach number of 0.6 are shown in Fig. 19. No wiggles are apparent in this plot, and the density residual history plot in Fig. 20 shows a three order-of-magnitude convergence in 1200 time steps. There is a slight lack of symmetry in the contours, but this is quite typical of low-order solutions.

IV. Concluding Remarks

Our ultimate goal is to set down a high-order accurate grid-independent algorithm. The method described in this paper is a rational first step toward this goal. The results shown earlier demonstrate the viability of the basic approach we have adopted; although less than second-order accurate, the algorithm provides remarkably high resolution solutions. The manner in which the flux function should be modified to recover a second-order accurate scheme is currently being investigated. We also continue to seek improvements in two important areas: strong-wave transitions are not strictly monotonic, and solutions fail to converge to machine zero. The importance of these issues is likely to grow as the order of accuracy of the method is increased. Therefore, although the present method represents a substantial improvement over the earlier grid-independent schemes, we continue to search for ways to further enhance monotonicity and convergence.

Acknowledgment

This research was supported in part by NASA Langley Research Center under research Grant NAG-1-1207, with James D. Keller, technical officer.

References

[1]Parpia, I. H., and Michalek, D. J., "A Shock Capturing Method for Multidimensional Flow," AIAA Paper 90-3016, Aug. 1990

[2]Rumsey, C. L., van Leer, B., and Roe, P. L., "A Grid-Independent Approximate Riemann Solver with Applications to the Euler and Navier-Stokes Equations," AIAA Paper 91-0239, Jan. 1991.

[3]Rumsey, C. L., van Leer, B., and Roe, P. L., "Effect of a Multidimensional Flux Function on the Monotonicity of Euler and Navier-Stokes Computations," AIAA Paper 91-1530-CP, June 1991.

[4]Parpia, I., "A Planar Oblique Wave Model for the Euler Equations," AIAA Paper 91-1545-CP, June 1991.

[5]Roe, P. L., "Discrete Models for the Numerical Analysis of Time-Dependent Multidimensional Gasdynamics," *Journal of Computational Physics*, Vol. 63, No. 2, 1986, pp. 458–476.

[6]Hase, J. E., Anderson, D. A., and Parpia, I., "A Delaunay Triangulation Method and Euler Solver for Bodies in Relative Motion," AIAA Paper 91-1590-CP, June 1991.

[7]Roe, P. L., "Approximate Riemann Solvers, Parameter Vectors, and Difference Schemes," *Journal of Computational Physics*, Vol. 43, No. 2, 1981, pp. 357–372.

[8]Struijs, R., Deconinck, H., de Palma, P., Roe, P., and Powell, K. G., "Progress on Multidimensional Upwind Euler Solvers for Unstructured Grids," AIAA Paper 91-1550-CP, June 1991.

[9]Kentzer, C. P., "Quasi-Linear Form for the Rankine-Hugoniot Jump Conditions," *AIAA Journal*, Vol. 24, No. 4, 1986, pp. 691–692.

[10]Levy, D. W., Powell, K. G., and van Leer, B., "An Implementation of a Grid-Independent Upwind Scheme for the Euler Equations," AIAA Paper 89-1931, June 1989.

[11]Chakravarthy, S., and Osher, S., "Numerical Experiments with the Osher Upwind Scheme for the Euler Equations," *AIAA Journal*, Vol. 2, No. 9, 1983, pp. 1241–1248.

[12]Michalek, D. J., "An Investigation of Genuinely-Multidimensional Schemes for the Euler Equations," Ph.D. Dissertation, Dept. of Aerospace Engineering, Univ. of Texas at Arlington, Arlington, TX, May 1992.

[13]Barth, T. J., and Jesperson, D. C., "The Design and Application of Upwind Schemes on Unstructured Meshes," AIAA Paper 89-0366, Jan. 1989.

[14]Barth, T. J., "A 3-D Upwind Euler Solver for Unstructured Meshes," AIAA Paper 91-1548-CP, June 1991.